AD-A139 769 A SECOND ORDER UPWIND FLUX METHOD FOR HYPERBOLIC CONSERVATION LAWS(U) NAVAL OCEAN RESEARCH AND DEVELOPMENT ACTIVITY NSTL STATION MS B E MCDONALD 1/1

UNCLASSIFIED NOV 83 NORDA-57 F/G 20/4 NL

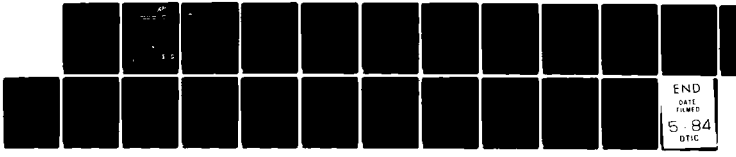

END
DATE FILMED
5-84
DTIC

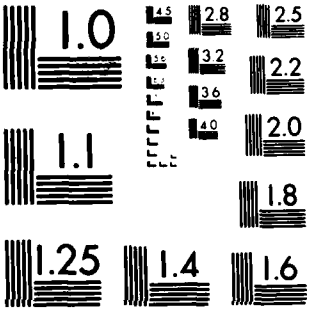

NORDA Report 57

A Second Order Upwind Flux Method for Hyperbolic Conservation Laws

B. Edward McDonald

Numerical Modeling Division
Ocean Science and Technology Laboratory

November 1983

Naval Ocean Research and Development Activity
NSTL, Mississippi 39529

The advancing state of the art in computing technology and numerical methods brings increasingly difficult scientific problems into active investigation. Some of these problems, in turn, challenge the capabilities of existing numerical techniques and stimulate development of new ones. In 1981 the Office of Naval Research put forth a call to two national laboratories for further involvement in a longstanding problem in wave propagation theory: the behavior of a nonlinear pulse incident on a caustic surface. This had been an unresolved issue in the aircraft-generated sonic boom studies of the 1970s. It is currently an issue in the oceanic nuclear standoff problem. Experimentation with existing methods for nonlinear hyperbolic systems and shock waves prompted development of the numerical technique presented here. Both in its present form and in future refinements this technique can be of value in other areas. Examples of naval interest are broadband pulse propagation, surface and internal waves, and ocean circulation.

G. T. Phelps, Captain, USN
Commanding Officer, NORDA

Executive Summary

We present first- and second-order upwind schemes employing a numerically calculated characteristic speed direction and combine them into a simple monotonicity preserving hybrid scheme using the method of flux correction. The first-order scheme is constructed to maintain accuracy at flow reversal points. The hybrid scheme computes a provisional update from the first-order scheme, and then filters the second-order corrections to prevent occurrence of new extrema. We derive analytic solutions for a developing N-wave shock, and compare computed versus analytic results for two different N waves and for a third case involving linear advection of a square wave. Results are given with and without the second-order correction. The second-order results are always superior to first-order results, with the most dramatic difference occurring for the case of linear advection. The results suggest that higher order differences could be substituted in the hybrid scheme to reduce truncation error even further.

Acknowledgments

This work was supported during FY-83 by the Office of Naval Research under Program Element 61153N. The project manager was Peter Rogers.

Contents and Illustrations

Contents

Illustrations

A Second Order Upwind Flux Method for Hyperbolic Conservation Laws

1. Introduction

The development of flow discontinuities in hyperbolic systems presents substantial difficulties to finite difference solution algorithms. First-order upwind differences taken in the direction of the characteristic speed alleviate artificial oscillations near a shock at the expense of adding, implicitly or explicitly, artificial dissipation. The flux correction approach of Zalesak (1979) addresses this problem through construction of a hybrid scheme that results in high-order centered differences being used where the flow is smooth, and one-sided differences being used near discontinuities.

Although this method is capable of producing impressive results for initial conditions containing shocks (Zalesak, 1981), it generates shocks too rapidly in some cases where they evolve from continuous initial conditions. Here we demonstrate that the flux correction technique enables the use of spatially high-order upwind differencing while maintaining proper monotonicity constraints. We show that a hybrid scheme consisting of first- and second-order upwind differences in tandem results in excellent agreement between analytic and numerical solutions for a steepening N-wave shock--a familiar phenomenon in nonlinear acoustics. The scheme presented here is under continued investigation to remove expansion shocks (time-reversed shocks forbidden by the second law of thermodynamics) and a mild amplification of long wavelength modes.

We wish to distinguish between the approach taken here and that taken in contemporary versions of the scheme of Godunov (1959). These schemes are reviewed by van Leer (1981) and by Harten, et al. (1983). These schemes view flow variables as piecewise constant, so that a continuous variation becomes the limit of vanishingly small stepwise variations. Time advancement is achieved by invoking exact or approximate solutions of the individual noninteracting shock problems (i.e., the Riemann problem for Burgers' equation) for a small increment of time δt. A new stepwise representation is then recovered by spatial averaging. This approach has advantages when the flow consists of clean, well-formed shocks. However, in regions where the flow is dominated by linear advection, the results are highly dissipative, as with the first-order upwind method.

Here we present the first- and second-order upwind methods, derive an analytic model for a steepening N-wave shock, and compare numerical versus analytic results for this model and for the linear advection of a square wave. The first-order method differs from others in current use by employing a characteristic speed calculated internally from point values of flux and the variable of integration (density or velocity). It is also independent of any specific model such as Burgers' equation.

In Section 2 we present equations and conservation laws that motivate our approach. Section 3 derives analytic models for validation of the numerical results. Section 4 presents the numerical methods to be used, and shows the first-order scheme to be monotone for all flow conditions as long as the Courant condition is satisfied. Section 5 then compares analytic and numerical

results for the second-order corrected scheme and for the first-order scheme alone.

2.0 Equations and Conservation Laws

We are concerned with hyperbolic systems which can be modeled by the scalar initial value problem

$$\rho_t + \phi(\rho)_x = 0, \tag{1a}$$

$$\rho(x,0) = \rho_0(x), \tag{1b}$$

where the flux ϕ is a smooth function of ρ.

The variable ϕ in various applications may play the role of a mass density, a density perturbation (as in the nonlinear acoustics problem which motivated this work), or a velocity variable. Thus, in general, ρ may take on positive or negative values.

The method developed here is intended for systems more general than Eq. (1), with source terms and coupling to other variables. For the moment, however, we use well-known properties of Eq. (1) including analytic solutions as a test of the numerics. Equation (1a) may be expressed

$$\rho_t + u(\rho)\,\rho_x = 0, \tag{2}$$

where $u(\rho) = \phi_\rho$ (3)

is known as the characteristic speed. Equation (2) implies preservation of monotonicity: $\rho_t = 0$ at local extrema.

It is also worth noting that prior to shock formation, Eq. (1a) implies under a variety of boundary conditions that all moments of the distribution ρ are constant:

$$\frac{\partial}{\partial t}\int \rho^m dx = 0, \quad m = 1, 2, 3 \ldots \tag{4}$$

Depending upon the form of the flux and the initial condition, Eq. (2) may admit analytic solutions up to the formation of a shock. These are found as follows. Equation (2) implies constancy of ρ along the trajectory

$$x_t = u(\rho). \tag{5}$$

Both x_t and u are constant on this trajectory, so the value of ρ at (x,t) may be found by mapping back to the initial condition:

$$\rho(x,t) = \rho_0(x - t\,u(\rho)). \tag{6}$$

Analytic solutions are generated by solving Eq. (6) for ρ in terms of x and t. In an example to be given in Section 3, $u(\rho)$ is taken to be linear and $\rho_0(x)$ quadratic. Then $\rho(x,t)$ emerges as the solution of a quadratic equation.

After sufficient time the characteristics (Eq. (5)) for neighboring points of an initial distribution may cross, leading to mathematical solutions which are multivalued. These mathematical solutions still maintain monotonicity and constancy of all moments in Eq. (4), but loose physical meaning. Physically, an arbitrarily small amount of viscosity becomes dominant as $|\rho_x|$ approaches infinity, and a shock is formed. From that time forward, only the fundamental moment (m=1 in Eq. (4)) is preserved. This corresponds to conservation of mass or momentum, depending upon the interpretation of the variable ρ. To illustrate this point, we will derive the Rankine-Hugoniot relation as follows. Consider a discontinuous profile with constant left and right states:

$$\rho = \rho_L + (\rho_R - \rho_L)\, H(x-vt) \qquad (7)$$

$$\phi(\rho) = \phi_L + (\phi_R - \phi_L)\, H(x-vt), \qquad (8)$$

where

$$H(x) = \begin{cases} 1, & x>0 \\ 0, & x<0, \end{cases} \qquad (9)$$

and v is the shock propagation speed. Substituting Eqs. (7)-(9) into Eq. (1a) and equating coefficients of $H(x)_x = \delta(x)$ gives the Rankine-Hugoniot relation

$$v(\rho_L - \rho_R) = \phi_L - \phi_R \,. \qquad (10)$$

Generalizing Eqs. (7)-(10), a propagation speed v_m could be defined by imposing conservation of the quantity ρ^m across the shock. Eqs. (1a) and (3) give

$$\frac{\partial}{\partial t}\, \rho^m + m\, \frac{\partial}{\partial x} \int^{\rho} u(\rho)\, \rho^{m-1}\, d\rho = 0, \qquad (11)$$

and Eqs. (7)-(10) generalize to

$$v_m \left(\rho_L^m - \rho_R^m\right) = m \int_{\rho_R}^{\rho_L} \rho^{m-1}\, u(\rho)\, d\rho \,. \qquad (12)$$

Unless u = constant, corresponding to linear advection at a constant velocity, preservation of each moment would require a different propagation speed. Conservation of mass (or momentum, depending upon the interpretation of ρ) is absolutely essential, so Eq. (10) wins out in the determination of the shock speed.

It is important to note that flux conservation (Eq. (1a)) is sufficient to yield the proper shock speed. This will be exploited in the numerical scheme to be constructed below. In particular, the numerics are cast in flux conservative form, with no distinction between shocks and steep but continuous profiles. The emergence of a shock with proper speed from a steepening continuous profile then serves to validate the method.

3.0 Analytic Models

In this section we present two analytic models to be used as benchmarks for the numerical algorithms. The first is a folded parabolic lobe (approximating one cycle of a sine wave) that evolves nonlinearly to an N-wave shock. The second is the linear advection of a square wave in a constant velocity field--a problem posed by Boris and Book (1973) and used frequently to demonstrate the flux correction technique.

Let us consider an inviscid Burgers' equation cast in a moving frame of reference:

$$\rho_t + \left(\frac{a}{2}\, \rho^2 - u_0 \rho\right)_x = 0, \qquad (13)$$

where a and u_0 are constants. The u_0 term is added to demonstrate the numerics' robustness against formation of nonphysical "expansion shocks." Let the initial condition be

$$\rho_0(x) = \max\left(0,\, bx\,(x_0 - x)\right), x \geq 0 \qquad (14)$$

and

$$\rho_0(-x) = -\rho_0(x). \qquad (15)$$

The result is a pair of antisymmetric parabolic lobes shown in Figure 1.

Within each lobe, an analytic solution can be found from Eq. (6). From Eqs. (13) and (1a),

$$u = a\rho - u_o , \tag{16}$$

so the equation to be solved is

$$\rho = b\left[x_o\,(x - t(a\rho - u_o)) - (x - t(a\rho - u_o))^2 \right] . \tag{17}$$

The solution which has the proper form for $t \to 0$ is

$$\rho = (x + u_o t - q)/at \tag{18}$$

where

$$q = 1/2\left(x_o + \frac{1}{abt}\right) - \left[1/4\left(x_o + \frac{1}{abt}\right)^2 - \frac{x + u_o t}{abt}\right]^{\frac{1}{2}} . \tag{19}$$

This mathematical solution is physically valid for $0 < t < (abx_o)^{-1}$ and $0 \leqslant x + u_o t \leqslant x_o$.

We generate the negative lobe by folding:

$$\rho(-x-u_o t,\, t) = -\,\rho(x+u_o t,\, t). \tag{20}$$

For $t>(abx_o)^{-1}$, the mathematical solution is multivalued, with Eq. (19) joining at a branch point onto the corresponding root with positive radical. The physical solution, however, follows Eq. (19) out to the point at which the area under the positive lobe equals that of the initial condition, and then drops discontinuously to zero. The shock location x_s can be determined analytically by setting

$$\int_{-u_o t}^{x_s} \rho(x,t)\,dx = \int_0^{x_o} \rho(x,0)\,dx . \tag{21}$$

From Eqs. (14), (18), and (19) this gives

$$\frac{x_o^3}{6abt} = \frac{x'^2}{2} - \frac{x'}{2}\left(x_o + \frac{1}{abt}\right) - \frac{2}{3}\,abt\left[\frac{1}{4}\left(x_o + \frac{1}{abt}\right)^2 - \frac{x'}{abt}\right]^{3/2} + \frac{abt}{12}\left(x_o + \frac{1}{abt}\right)^3 , \tag{22}$$

where $x' = x + u_o t$. (23)

Even though $x'=x_o$ satisfies Eq. (21) for all $t>0$, it does not give the shock location. This root holds for the steepening phase of the physical solution, and after shock formation it applies only to the double valued mathematical solution. Shock formation occurs when the radical in Eq. (19) first vanishes on the interval $0<x'<x_o$. This occurs at $(x',t) = (x_o, (abx_o)^{-1})$. Eq. (22) yields a quartic equation for x', that may be reduced to a quadratic by removal of the double root $x'=x_o$. Of the two remaining roots, the one corresponding to a rightward progressing shock is

$$x_s = -u_o t + \frac{1}{9abt} + \left(\frac{abt}{3}\right)^{1/2}\left(x_o + \frac{1}{3abt}\right)^{3/2}. \quad (24)$$

In summary, the parabolic lobe analytic solution consists of: $\rho = 0$ for $x > x_s$; Eqs. (18) and (19) for $-u_o t < x < x_s$; and Eq. (20) for $x < -u_o t$.

The second analytic solution to be used in numerical tests is that of a square wave moving at a constant velocity u_o:

$$\rho = \begin{cases} 1, & 0 \leq x + u_o t \leq x_o \\ 0 & \text{otherwise.} \end{cases} \quad (25)$$

This simple case will serve to illustrate effects of diffusion and dispersion in the numerical algorithms.

4.0 Numerical Techniques

We present two separate upwind difference schemes and combine them in a hybrid scheme by the method of flux correction (Zalesak, 1979). For simplicity we assume a constant grid interval δx. We take ρ_i and ϕ_i to be values at integer grid points, and define half integer grid point variables $f_{i+1/2}$ and $w_{i+1/2}$. Here f is a numerical flux to be specified below and w is the sign of the characteristic speed (whose only purpose is to define the upwind direction). In practice we take

$$w_{i+1/2} = (\phi_{i+1} - \phi_i)*(\rho_{i+1} - \rho_i). \quad (26)$$

Note we have replaced the division in a second order representation u in Eq. (3) by a multiplication. This results in w being of the proper sign, while saving computer time and avoiding the risk of a zero divide.

4.1 The First-Order Scheme

A representation of Eq. (1a), which is first-order and which reduces to the familiar upwind scheme in the case of constant flow velocity, is as follows:

$$\rho_i^{n+1} - \rho_i^n = - f_{i+1/2} + f_{i-1/2}, \quad (27)$$

where the superscript indicates the time level ($t = n\delta t$) and

$$f_{i+1/2} = \begin{cases} \phi_i \ \delta t/\delta x, & w_{i+1/2} \geq 0 \\ \phi_{i+1} \ \delta t/\delta x, & w_{i+1/2} < 0. \end{cases} \quad (28)$$

The distinction between this scheme and ordinary upwind lies in the explicit prescription Eqs. (26)-(28) for the upstream direction in terms of point values of ϕ and ρ as opposed to the characteristic speed u or the flow speed v.

Quantities without superscripts are evaluated at time level n. The above scheme preserves monotonicity, as shown by consideration of the following four cases:

Case 1. $w_{i-1/2} \geq 0$, $w_{i+1/2} \geq 0$.

Eqs. (27) and (28) give

$$\rho_i^{n+1} - \rho_i^n = - \delta t/\delta x \ (\phi_i - \phi_{i-1}) \quad (29)$$

$$= - \delta t/\delta x \ \bar{u}_-(\rho_i - \rho_{i-1}) \quad (30)$$

where

$$\bar{u}_- = (\phi_i - \phi_{i-1})/(\rho_i - \rho_{i-1}) = u(\bar{\rho}_-). \quad (31)$$

The last identity results from the mean value theorem, with $\bar{\rho}_-$ lying in the interval (ρ_i, ρ_{i-1}). Then

$$\rho_i^{n+1} = \rho_i (1 - \varepsilon_-) + \rho_{i-1} \varepsilon_- , \quad (32)$$

where

$$\varepsilon_- = |\bar{u}_- \delta t/\delta x| . \quad (33)$$

Even though $\bar{u}_-$ is positive in this case, we retain the absolute value in Eq. (33) for convenience below. Eq. (32) demonstrates that monotonicity is preserved for $\varepsilon \leqslant 1$. Specifically, the right-hand side of Eq. (32) consists of a weighted mean of neighboring ρ values, with each weight being non-negative for $\varepsilon \leqslant 1$.

Case 2. $w_{i-1/2} < 0$, $w_{i+1/2} < 0$.

As above, we find

$$\rho_i^{n+1} = \rho_i (1 - \varepsilon_+) + \rho_{i+1} \varepsilon_+ , \quad (34)$$

where

$$\varepsilon_+ = |\bar{u}_+ \delta t/\delta x|, \quad (35)$$

and

$$\bar{u}_+ = (\phi_{i+1} - \phi_i)/(\rho_{i+1} - \rho_i) = u(\bar{\rho}_+), \quad (36)$$

with $\bar{\rho}_+$ lying on the interval (ρ_{i+1}, ρ_i). Monotonicity is preserved in this case for $\varepsilon_+ \leqslant 1$.

Case 3. $w_{i - 1/2} < 0$, $w_{i + 1/2} > 0$

Eqs. (27) and (28) yield

$$\rho_i^{n+1} = \rho_i \quad (37)$$

This reflects that u=0 within one cell of point i.

Case 4. $w_{i - 1/2} > 0$, $w_{i + 1/2} < 0$

The straightforward result from Eqs. (27) and (28) gives

$$\rho_i^{n+1} - \rho_i = -\delta t/\delta x (\phi_{i+1} - \phi_{i-1}). \quad (38)$$

A small amount of manipulation after adding and subtracting ϕ_i within the parentheses yields

$$\rho_i^{n+1} = \rho_i (1-\varepsilon_- - \varepsilon_+) + \rho_{i+1} \varepsilon_+ + \rho_{i-1} \varepsilon_- . \quad (39)$$

This case provides the most stringent condition on monotonicity (and thus stability as well):

$$|u\ \delta t/\delta x| < 1/2\ . \tag{40}$$

4.2 The Higher-Order Scheme

A one-sided representation of Eq. (1a) that has second-order spatial accuracy is

$$\rho_i^{n+1} - \rho_i^n = -\ \delta t/\delta x\ (3/2\ \phi_i - 2\phi_{i-1} + 1/2\phi_{i-2}). \tag{41}$$

This representation has higher-order accuracy than the first-order scheme Eqs. (26)-(28), but is of little interest by itself because it does not preserve monotonicity. Under the assumption that the characteristic speed is locally constant, the stability condition for Eq. (41) at high wavenumbers is

$$|u\ \delta t/\delta x| \leq 1/2\ , \tag{42}$$

which coincides with Eq. (40). Note that the first-order analog of Eq. (41) is

$$\rho_i^{n+1} - \rho_i^n = -\ \delta t/\delta x\ (\phi_i - \phi_{i-1})\ . \tag{43}$$

By comparison of Eqs. (43) and (41) we construct numerical fluxes for the second-order scheme as follows:

$$F_{i+1/2} = 3/2\ f_{i+1/2} - 1/2\ S_{i+1/2}\ , \tag{44}$$

where

$$S_{i+1/2} = \begin{cases} f_{i-1/2}\ , & w_{i+1/2} \geq 0 \\ f_{i+3/2}\ , & w_{i+1/2} < 0. \end{cases} \tag{45}$$

The generalization of Eq. (41) is then

$$\rho_i^{n+1} - \rho_i^n = -F_{i+1/2} + F_{i-1/2} \tag{46}$$

In practice, F is constructed according to Eqs. (44) and (45), but Eq. (46) is replaced by the hybrid scheme to follow.

4.3 The Hybrid Scheme

Following Zalesak (1979) we construct the following provisional quantities:

$$\rho_i^* = \rho_i^n - f_{i+1/2} + f_{i-1/2} \tag{47}$$

$$\delta f_{i+1/2} = F_{i+1/2} - f_{i+1/2}\ . \tag{48}$$

We now have a first-order update ρ^* in which monotonicity has been preserved. Next, we perform a "flux correction" before completing the update. This is simply a filtering operation that forbids higher-order enhancement of extrema. For simplicity we use the original form of Boris and Book (1973):

$$\delta f_{i+1/2} \rightarrow s_{i+1/2} \max\Big(0, \min\Big[|\delta f_{i+1/2}|,\ s_{i+1/2}\,(\rho^*_{i+2} - \rho^*_{i+1})\ ,\ s_{i+1/2}\,(\rho^*_i - \rho^*_{i-1})\Big]\Big)\ , \tag{49}$$

where

$$s_{i+1/2} = \begin{cases} 1, & \delta f_{i+1/2} \geq 0 \\ -1, & \delta f_{i+1/2} < 0 \end{cases} . \quad (50)$$

Innovations to the above, including extension to multidimensions without timestep splitting, have been given by Zalesak (1979).

The hybrid scheme is completed as follows:

$$\rho_i^{n+1} = \rho_i^n - \delta f_{i+1/2} + \delta f_{i-1/2} . \quad (51)$$

One advantage of the above hybrid scheme over schemes involving piecewise-analytic solutions is its programming simplicity. The subroutine that executes the entire hybrid scheme, Eqs. (27-51), consists of 29 executable Fortran statements, of which six are calls to an endpoint setting routine of length six statements (see the Appendix). A second advantage is that the scheme itself is independent of the specific relation between ϕ and ρ (i.e., Burgers' equation or whatever).

5.0 Numerical Results

In this section we present calculations for three examples in which exact results are known. Each is based on results given in Section 3. The first is the development of an N-wave shock in which positive and negative lobes produce an antisymmetric velocity distribution (i.e., $u_o \neq 0$ in Eq. (13)). Second is the development of an N wave in drifting frame ($u_o \neq 0$). The motivation for this case is to demonstrate that expansion shocks do not result where $u = 0$, $\rho \neq 0$ and $u_x > 0$. We noted that they did occur under these circumstances where the flow speed, rather than the characteristic speed, was used to determine the upwind direction. The third case is the passive advection of square wave profile. This example illustrates most clearly the gains achieved through higher order flux correction. All examples use a mesh of 202 points spaced at equal intervals. The two endpoints are reset after each calculation using periodic boundary conditions. The timestep is constant for each case, resulting in Courant numbers $|u|_{max} \delta t/\delta x$ as given below.

Example 1.

Initial conditions are taken from Eqs. (14) and (15). Time advancement is achieved by defining

$$\phi_i = a/2\ \rho_i^2 - u_o \rho_i \quad (52)$$

as in Eq. (13) (with $u_o = 0$ in this case) prior to executing the hybrid scheme of Section 4. The timestep is such that the maximum Courant number is

$$ab\ x_o^2\ \delta t/4\delta x = 1/4. \quad (53)$$

Figure 1 shows the initial condition followed by results from the first-order scheme and results from the hybrid scheme. Parameters are such that the shock forms at step 41. After this point in time, the second-order correction shows increasing improvement over the purely first-order result. Note that the second-order method at step 601 shows clear superiority in locating the shock properly and maintaining its sharpness.

Example 2.

Initial conditions are the same as in example 1, but a drift term $u_o \neq 0$ is present in Eq. (52). The timestep is the same as in example 1, but the

presence of the drift term raises the Courant number from 0.25 to 0.3375. The value of u_o is such that u = 0, where is equal to 0.35 of its initial maximum value. As shown in Figure 2, the profiles remain smooth at this value, demonstrating stability against nonphysical expansion shocks. Tests run with higher values of u_o have also confirmed this point. In tests using the local flow speed $v = 1/2a\rho - u_o$ rather than u to determine the upwind direction, expansion shocks did occur where v = 0 and $v_x > 0$. Comparison of the first-order portions of Figures 1 and 2 illustrates the first-order scheme's increasing dissipation with increasing Courant number. The second-order results, however, are much less subject to this type of error. The steplike structure at step 601 is simply a result of the periodic boundary conditions used here.

Example 3.

The square wave profile shown in Figure 3 is generated from Eq. (25). This test consists of linear advection with a courant number of 1/4. At the beginning of each step the flux is defined from Eq. (52) with a = 0. As the calculation proceeds, the first order results of Figure 3 show the initially sharp structure being progressively smoothed out. The second-order results, however, retain a much greater degree of fidelity to the analytic solution.

The results of Zalesak (1981) suggest that the residual dissipation present in the second-order results could be further reduced by employing higher-order upwind differences in the correction stage (44)-(51) of the hybrid scheme.

6.0 Conclusions

We have presented a simple first-order scheme for solving Eq. (1a) which maintains montonicity and avoids artificial expansion shock generation where the characteristic speed reverses sign. This is done without the use of artificial viscosity or Riemann solutions. We have also shown that the use of second-order upwind differences and the method of flux correction greatly reduce the dissipative effects of the first-order method while preserving monotonicity. The Rankine-Hugoniot relation for shock propagation speed is implicit in the method by virtue of flux conservation at the shock front. Comparisons of numerical and analytic results for a developing N-wave shock and for linear advection of a square wave confirm the accuracy of the method.

7.0 References

Boris, J. P. and D. L. Book (1973). Flux Corrected Transport 1. SHASTA, A Fluid Transport Algorithm That Works. J. Comput. Phys. v. 11, p. 38.

Godunov, S. K. (1959). A Difference Scheme for Numerical Computation of Discontinuous Solutions of Equations of Fluid Dynamics. Math. Sbornik, v. 47, p. 271.

Harten, A., P. D. Lax, and B. van Leer (1983). On Upstream Differencing and Godunov-Type Schemes for Hyperbolic Conservation Laws. SIAM Rev. v. 25, p. 35.

Harten, A. (1983). High Resolution Upwind Schemes. J. Comp. Phys. v. 49, p 357.

van Leer, B. (1981). On the Relation Between the Upwind-Differencing Schemes of Godunov. Enquist-Osher and Roe.

ICASE Report 81-11, NASA Langley Research Center.

Zalesak, S. T. (1979). Fully Multidimensional Flux-Corrected Transport Algorithms for Fluids. J. Comp. Phys. v. 31, p. 335.

Zalesak, S. T. (1981). Very High-Order and Pseudospectral Flux-Corrected Transport (FCT) Algorithms for Conservation Laws. Proc. Fourth IMACS International Symposium on Computer Methods for Partial Differential Equations. Lehigh Univ.

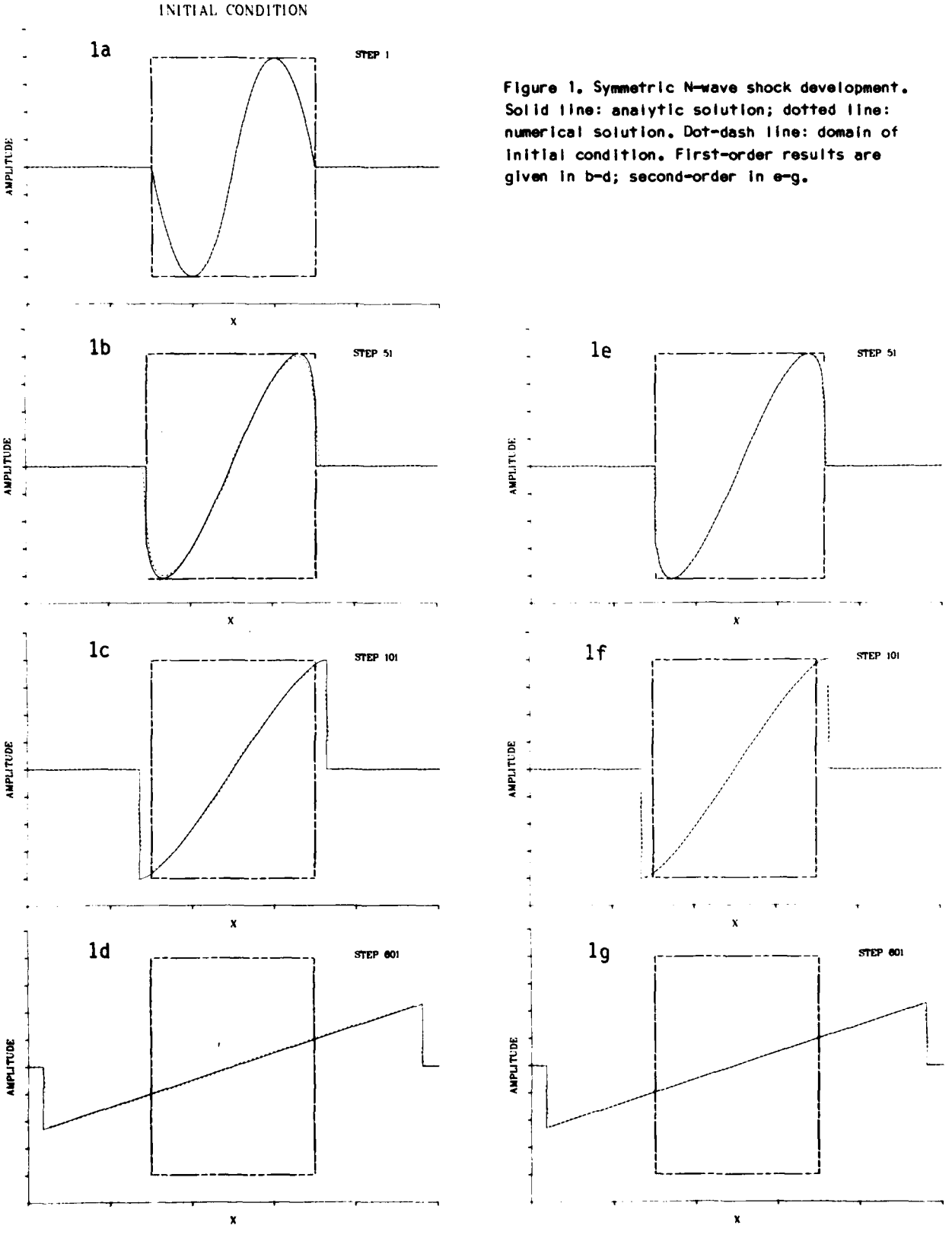

Figure 1. Symmetric N-wave shock development. Solid line: analytic solution; dotted line: numerical solution. Dot-dash line: domain of initial condition. First-order results are given in b-d; second-order in e-g.

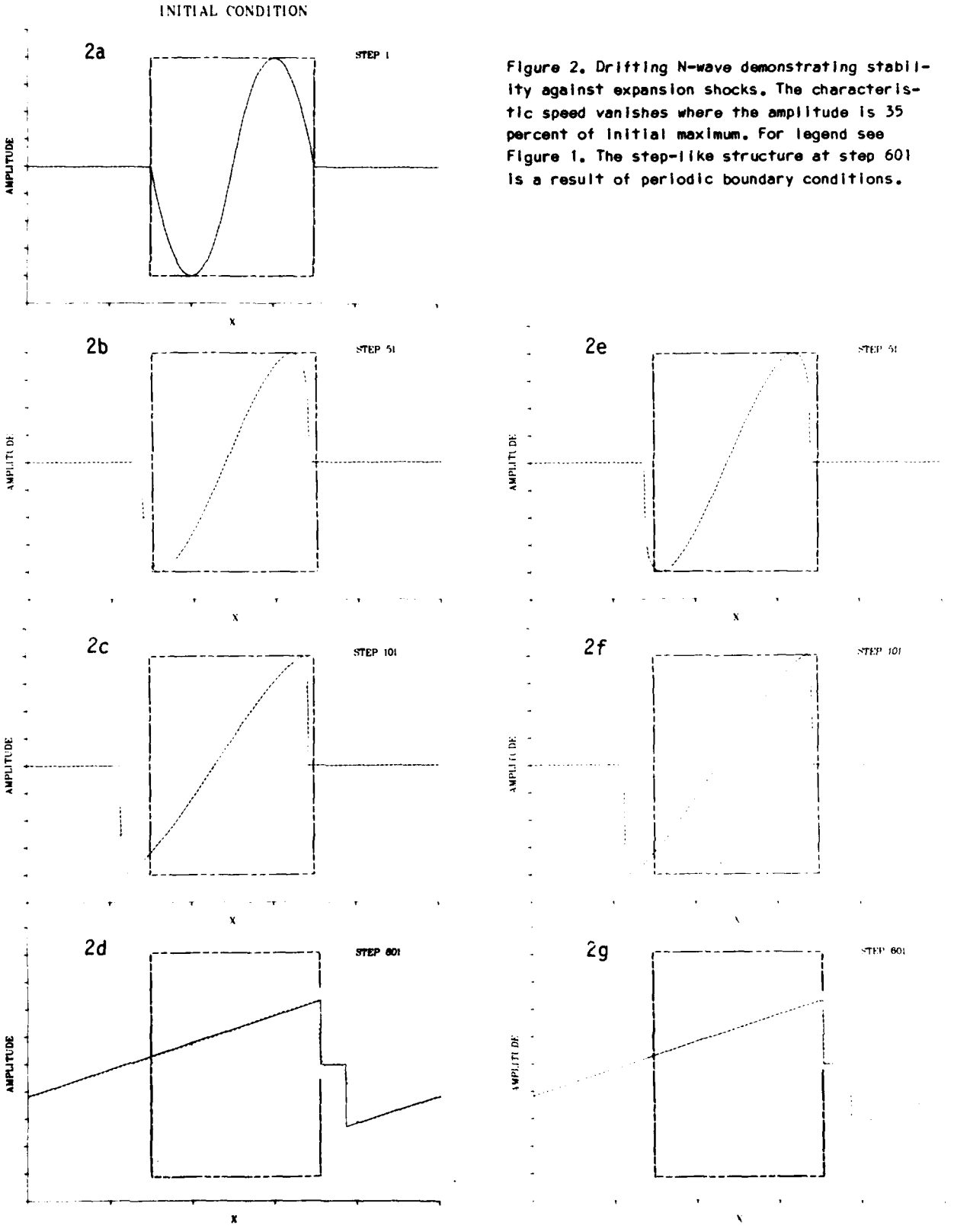

Figure 2. Drifting N-wave demonstrating stability against expansion shocks. The characteristic speed vanishes where the amplitude is 35 percent of initial maximum. For legend see Figure 1. The step-like structure at step 601 is a result of periodic boundary conditions.

Figure 3. Linear advection of a square wave. Solid line: exact solution; dashed line: numerical solution. First-order results appear in b-d; second in e-g.

Appendix: Fortran Statement Listing of the Upwind Flux Method Subroutine

```
      SUBROUTINE FLUX(N, PHI, F,S,W, R)
          REAL PHI(N), F(N), S(N), W(N), R(N)
C
C     VERSION OF MAY 1983
C     INTEGRATE FORWARD ONE TIMESTEP:    DR/DT = -D PHI/DX
C     1ST ORDER UPWIND ... FLUX CORRECTED TO 2ND ORDER.
C     PHI HAS BEEN NORMALIZED BY DT/DX IN THE CALLING PROGRAM.
C     SHORT WAVELENGTH STABILITY CRITERION IS U < .5,
C     WHERE U = D PHI/DR IS THE CHARACTERISTIC SPEED.
C
C     R AND PHI RESIDE AT INTEGER GRID POINTS AND MUST BE PREDEFINED.
C     FLUX VARIABLES F,S,W ARE SCRATCH ARRAYS RESIDING AT HALF INTEGER
C     GRID POINTS.  THE INDEXING CONVENTION IS
C         F(I) RESIDES AT I-.5    ... SAME FOR S AND W.
C
          NM = N-1
C
          DO 2 I=2,NM
          W(I) = (PHI(I) - PHI(I-1))*(R(I) - R(I-1))
          F(I) = PHI(I-1)
          IF(W(I) .LT. 0.) F(I) = PHI(I)
    2     CONTINUE
          CALL PBCSET(N, F)
C
          DO 3 I=2,NM
C     1ST ORDER UPDATE
          R(I) = R(I) - F(I+1) + F(I)
C
C     PREPARE 2ND ORDER CORRECTION
          F1 = F(I-1)
          IF(W(I) .LT. 0.) F1 = F(I+1)
    3     S(I) = .5*(F(I) - F1)
          CALL PBCSET(N,S)
          CALL PBCSET(N,R)
C
C     FLUX LIMITER
          DO 4 I=2,NM
          F(I) = SIGN(1., S(I))
    4     W(I) = R(I) - R(I-1)
          CALL PBCSET(N,W)
C
          DO 5 I=2,NM
    5     S(I) = F(I)*AMAX1(0.,AMIN1(ABS(S(I)),F(I)*W(I+1),F(I)*W(I-1)))
          CALL PBCSET(N, S)
C
C     FINAL CORRECTION
          DO 6 I=2,NM
    6     R(I) = R(I) - S(I+1) + S(I)
          CALL PBCSET(N, R)
      RETURN
      END

      SUBROUTINE PBCSET(N, A)
          REAL A(N)
C     SET PERIODIC BOUNDARIES
          A(1) = A(N-1)
          A(N) = A(2)
          RETURN
```

DISTRIBUTION LIST

Department of the Navy
Asst Deputy Chief of Navy Materials
for Laboratory Management
Rm 1062 Crystal Plaza Bldg 5
Washington DC 20360

Department of the Navy
Asst Secretary of the Navy
(Research Engineering & System)
Washington DC 20350

Project Manager
ASW Systems Project (PM-4)
Department of the Navy
Washington DC 20360

Department of the Navy
Chief of Naval Material
Washington DC 20360

Department of the Navy
Chief of Naval Operations
ATTN: OP 951
Washington DC 20350

Department of the Navy
Chief of Naval Operations
ATTN: OP 952
Washington DC 20350

Department of the Navy
Chief of Naval Operations
ATTN: OP 987
Washington DC 20350

Director
Chief of Naval Research
ONR Code 420
Ocean Science & Technology Det
NSTL, MS 39529

Director
Defense Technical Info Cen
Cameron Station
Alexandria VA 22314

Commander
DW Taylor Naval Ship R&D Cen
Bethesda MD 20084

Commanding Officer
Fleet Numerical Ocean Cen
Monterey CA 93940

Director
Korean Ocean R&D Inst
ATTN: K. S. Song, Librarian
P. O. Box 17 Yang Jae
Seoul South Korea

Commander
Naval Air Development Center
Warminster PA 18974

Commander
Naval Air Systems Command
Headquarters
Washington DC 20361

Commanding Officer
Naval Coastal Systems Center
Panama City FL 32407

Commander
Naval Electronic Sys Com
Headquarters
Washington DC 20360

Commanding Officer
Naval Environmental Prediction
Research Facility
Monterey CA 93940

Commander
Naval Facilities Eng Command
Headquarters
200 Stovall St.
Alexandria VA 22332

Commanding Officer
Naval Ocean R & D Activity
ATTN: Codes 110/111
Code 125
Code 200
Code 300
Code 115
Code 500
NSTL MS 39529

Director
Liaison Office
Naval Ocean R & D Activity
800 N. Quincy Street
502 Ballston Tower #1
Arlington VA 22217

Commander
Naval Ocean Systems Center
San Diego CA 92152

Commanding Officer
Naval Oceanographic Office
NSTL MS 39522

Commander
Naval Oceanography Command
NSTL MS 39522

Superintendent
Naval Postgraduate School
Monterey CA 93940

Commanding Officer
Naval Research Laboratory
Washington DC 20375

Commander
Naval Sea System Command
Headquarters
Washington DC 20362

Commander
Naval Surface Weapons Center
Dahlgren VA 22448

Commanding Officer
Naval Underwater Systems Center
ATTN: New London Lab
Newport RI 02840

Director
New Zealand Oceano Inst
ATTN: Library
P. O. Box 12-346
WELLINGTON N., NEW ZEALAND

Director
Office of Naval Research
Ocean Science & Technology Div
NSTL MS 39529

Department of the Navy
Office of Naval Research
ATTN: Code 102
800 N. Quincy St.
Arlington VA 22217

Commanding Officer
ONR Branch Office
536 S Clark Street
Chicago IL 60605

Commanding Officer
ONR Branch Office LONDON
Box 39
FPO New York 09510

Commanding Officer
ONR Western Regional Ofs
1030 E. Green Street
Pasadena CA 91106

President
Texas A&M
ATTN: Dept of Ocean Working Collection
College Station TX 77843

Director
University of California
Scripps Institute of Oceanography
P. O. Box 6049
San Diego Ca 92106

Director
Woods Hole Oceanographic Inst
Woods Hole MA 02543

UNCLASSIFIED

SECURITY CLASSIFICATION OF THIS PAGE *(When Data Entered)*

REPORT DOCUMENTATION PAGE	READ INSTRUCTIONS BEFORE COMPLETING FORM
1. REPORT NUMBER NORDA Report 57	2. GOVT ACCESSION NO. AD-A139769	3. RECIPIENT'S CATALOG NUMBER
4. TITLE *(and Subtitle)* A Second Order Upwind Flux Method for Hyperbolic Conservation Laws	5. TYPE OF REPORT & PERIOD COVERED Final
	6. PERFORMING ORG. REPORT NUMBER
7. AUTHOR(s) B. Edward McDonald	8. CONTRACT OR GRANT NUMBER(s)
9. PERFORMING ORGANIZATION NAME AND ADDRESS Naval Ocean Research and Development Activity Ocean Science and Technology Laboratory NSTL, Mississippi 39529	10. PROGRAM ELEMENT, PROJECT, TASK AREA & WORK UNIT NUMBERS 63785N
11. CONTROLLING OFFICE NAME AND ADDRESS Same	12. REPORT DATE November 1983
	13. NUMBER OF PAGES 22
14. MONITORING AGENCY NAME & ADDRESS(*if different from Controlling Office*)	15. SECURITY CLASS. *(of this report)* UNCLASSIFIED
	15a. DECLASSIFICATION DOWNGRADING SCHEDULE

16. DISTRIBUTION STATEMENT *(of this Report)*

Approved for Public Release
Distribution Unlimited

17. DISTRIBUTION STATEMENT *(of the abstract entered in Block 20, if different from Report)*

18. SUPPLEMENTARY NOTES

19. KEY WORDS *(Continue on reverse side if necessary and identify by block number)*

upward flux
hyperbolic conservation
N-wave shock
numerical modeling

20. ABSTRACT *(Continue on reverse side if necessary and identify by block number)*

We present first- and second-order upwind schemes employing a numerically calculated characteristic speed direction and combine them into a simple monotonicity preserving hybrid scheme using the method of flux correction. The first-order scheme is constructed to maintain accuracy at flow reversal points. The hybrid scheme computes a provisional update from the first-order scheme, and then filters the second-order corrections to prevent occurence of new extrema. We derive analytic solutions for a developing N-wave shock, and compare computed versus analytic results for two different N waves and for a

DD FORM 1 JAN 73 1473 EDITION OF 1 NOV 65 IS OBSOLETE
S/N 0102-LF-014-6601

UNCLASSIFIED
SECURITY CLASSIFICATION OF THIS PAGE *(When Data Entered)*

third case involving linear advection of a square wave. Results are given with and without the second-order correction. The second-order results are always superior to first-order results, with the most dramatic difference occurring for the case of linear advection. The results suggest that higher order differences could be substituted in the hybrid scheme to reduce truncation error even further.


8
TIC